



Cite this: *CrystEngComm*, 2023, 25, 4812

Realizing high performance bifunctional energy storage devices and electrocatalytic water splitting catalysts through regulated interface engineering of $\text{ZnCo}_2\text{O}_4@\text{Co}_3\text{O}_4$ nanosheets†

Lihua Miao,^a Lili Sui,^b Xiaoyan Shen,^a Dan Yang,^a He Huang^a and Ye Kuang^c

The development and optimization of electrocatalysts is one of the key points to reduce the energy barrier of electrocatalytic water splitting and improve the kinetics of electrocatalytic reactions. It is necessary to develop low-cost, high-performance electrocatalysts with large-scale application prospects. In order to solve this problem, hybrid structured $\text{ZnCo}_2\text{O}_4@\text{Co}_3\text{O}_4$ nanowires are successfully synthesized through hydrothermal synthesis and electrodeposition. As electrocatalysts for water splitting, $\text{ZnCo}_2\text{O}_4@\text{Co}_3\text{O}_4$ can reach a current density of 50 mA cm^{-2} at an overpotential of 278 mV for the OER and 166 mV@ -10 mA cm^{-2} for the HER, which could be higher than that of single ZnCo_2O_4 and Co_3O_4 . At the same time, $\text{ZnCo}_2\text{O}_4@\text{Co}_3\text{O}_4$ samples also exhibit a cell voltage of 1.67 V at a high current density of 50 mA cm^{-2} and superior durability for 50 h. The fabricated product also showcases a specific capacitance of 1316 F g^{-1} at 1 A g^{-1} . Additionally, the assembled device attains a maximum energy density of 47.3 W h kg^{-1} at a power density of 1126 W kg^{-1} . Furthermore, density functional theory (DFT) calculation further confirms that the heterostructure can significantly promote Gibbs free energy for hydrogen adsorption. And the significant increase in the density of total states (DOS) also enhances the catalytic activity for the HER.

Received 26th May 2023,
Accepted 13th July 2023

DOI: 10.1039/d3ce00534h

rsc.li/crystengcomm

Introduction

In recent decades, human society has been developing rapidly, and the accompanying energy shortages and environmental problems have made today's world face major challenges.^{1–3} Finding new green energy sources that can replace fossil fuels has become a very urgent and important task. So far, a variety of new energy sources have been developed and utilized.^{4,5} Among them, hydrogen energy has become one of the most promising alternative energy sources due to its high energy density and clean products.⁶ Among the variety of hydrogen production methods, electrolysis of water is the most simple and effective method.⁷ More electrons need to be transferred in the process of the oxygen evolution reaction, which makes it difficult to achieve mass production of hydrogen in practical application.⁸ The key to water electrolysis lies in the selection of electrode catalytic

materials. At present, commercial catalysts are mainly precious metals, but precious metals have low reserves and high cost.⁹ Thus, the development and optimization of electrocatalysts is one of the key points to reduce the energy barrier of electrocatalytic water splitting. Furthermore, supercapacitors, as an emerging energy storage technology, have attracted widespread attention.^{10–12} Compared to conventional batteries, supercapacitors offer higher energy density and faster charge–discharge rates, making them suitable for applications with high transient power

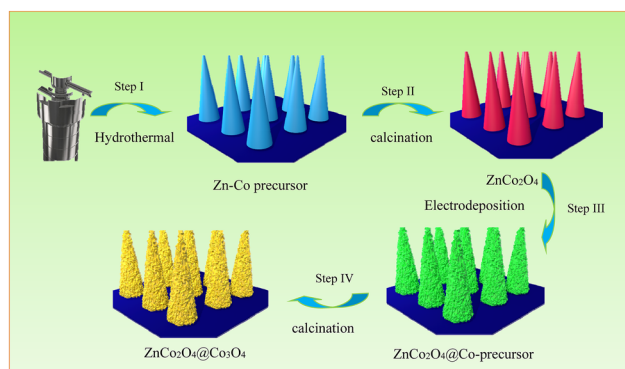


Fig. 1 Schematic diagram of the synthesis of the heterostructured $\text{ZnCo}_2\text{O}_4@\text{Co}_3\text{O}_4$ samples.

^a School of Medical Information Engineering, Shenyang Medical College, Shenyang 110043, Liaoning, China. E-mail: miaolihua@163.com

^b School of Pharmacy, Shenyang Medical College, Shenyang, 110043, Liaoning, China

^c Rare Earth Luminescence Materials, Shenyang Ligong University, Shenyang 110159, Liaoning, China

† Electronic supplementary information (ESI) available. See DOI: <https://doi.org/10.1039/d3ce00534h>

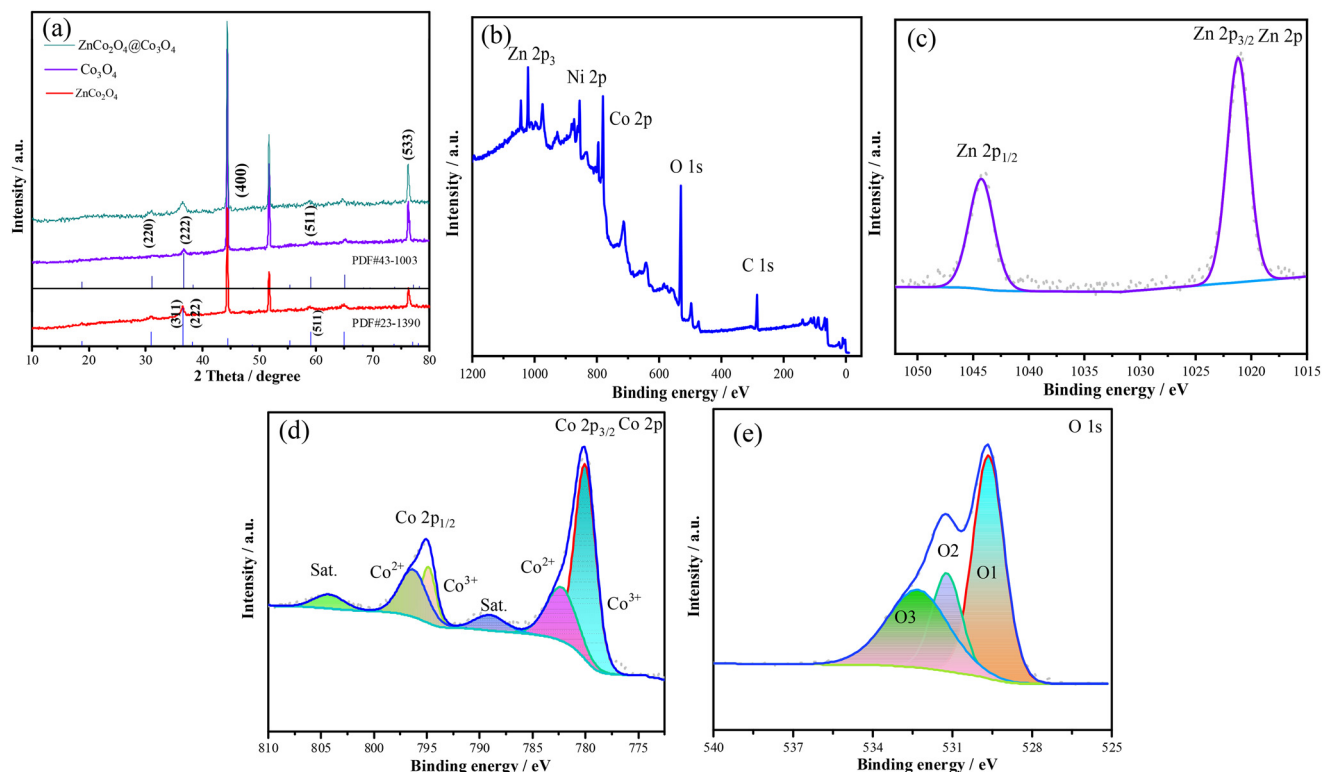


Fig. 2 (a) XRD patterns of the as-prepared samples, (b) the XPS survey spectra of $\text{ZnCo}_2\text{O}_4@\text{Co}_3\text{O}_4$, (c) Zn 2p XPS spectra, (d) Co 2p XPS spectra, and (e) O 1s XPS spectra.

demands.¹³ They can serve as power sources for electric vehicles, overcoming the limitations of long charging times and short driving ranges associated with traditional batteries.

In recent years, a lot of research work has shown that non-precious metal-based catalysts have special electronic structure, good catalytic performance, abundant reserves, and easy preparation and regulation, which can greatly reduce production costs and difficulties, showing their application prospects.¹⁴ Among them, ZnCo_2O_4 is a promising candidate due to its excellent electrocatalytic properties, modified spinel structure and higher conductivity compared to single-metal oxides,^{15–17} which leads to good electron transport ability and can effectively promote the efficiency of catalytic reaction, and has become one of the popular research materials. In addition, ZnCo_2O_4 nanostructures can also be used as catalysts for water electrolysis.^{18–20} However, the ZnCo_2O_4 material also has the problem of the volume being prone to drastic changes during the reaction.^{21,22} Therefore, a reasonable preparation method needs to be designed to improve the material. Furthermore, researchers have found that Co_3O_4 has a unique property where its Co ion can improve the conductivity and catalytic activity.^{23,24} This inspired us to combine the advantages of ZnCo_2O_4 and Co_3O_4 to design highly efficient $\text{ZnCo}_2\text{O}_4@\text{Co}_3\text{O}_4$ nanowires for energy conversion fields.

Herein, we synthesized ZnCo_2O_4 -based NWAs grown on Ni foam substrates through simple hydrothermal synthesis and electrodeposition and subsequent heat treatment strategies.

As electrocatalysts for water splitting, $\text{ZnCo}_2\text{O}_4@\text{Co}_3\text{O}_4$ can reach a current density of 50 mA cm^{-2} with an overpotential of 278 mV and a Tafel slope of 67.6 mV dec^{-1} for the OER, and an overpotential of 166 mV and a Tafel slope of $106.4 \text{ mV dec}^{-1}$ for the HER, which could be higher than that of single ZnCo_2O_4 and Co_3O_4 . At the same time, $\text{ZnCo}_2\text{O}_4@\text{Co}_3\text{O}_4$ samples also exhibit a cell voltage of 1.67 V and superior durability for 50 h. The fabricated product also shows a specific capacitance of 1316 F g^{-1} at 1 A g^{-1} . This means that the heterogeneous structure can realize the structure optimization of ZnCo_2O_4 electrocatalysts and improve the corresponding electrochemical performance.

Results and discussion

The preparation process of the heterostructure $\text{ZnCo}_2\text{O}_4@\text{Co}_3\text{O}_4$ is shown in Fig. 1. First, various raw materials and pretreated nickel foam were put into the reactor and the corresponding precursors were obtained by a hydrothermal method. Subsequent calcination treatment converts the precursor into the ZnCo_2O_4 product. Next, a layer of $\text{Co}(\text{OH})_2$ was deposited on the surface of the ZnCo_2O_4 sample by electrodeposition. Finally, the $\text{ZnCo}_2\text{O}_4@\text{Co}(\text{OH})_2$ product was thermally treated to convert $\text{Co}(\text{OH})_2$ into Co_3O_4 samples. Then the heterostructures of $\text{ZnCo}_2\text{O}_4@\text{Co}_3\text{O}_4$ nanocomposites were obtained.

Through XRD, ZnCo_2O_4 , Co_3O_4 and $\text{ZnCo}_2\text{O}_4@\text{Co}_3\text{O}_4$ phase structures were observed. Three strong peaks

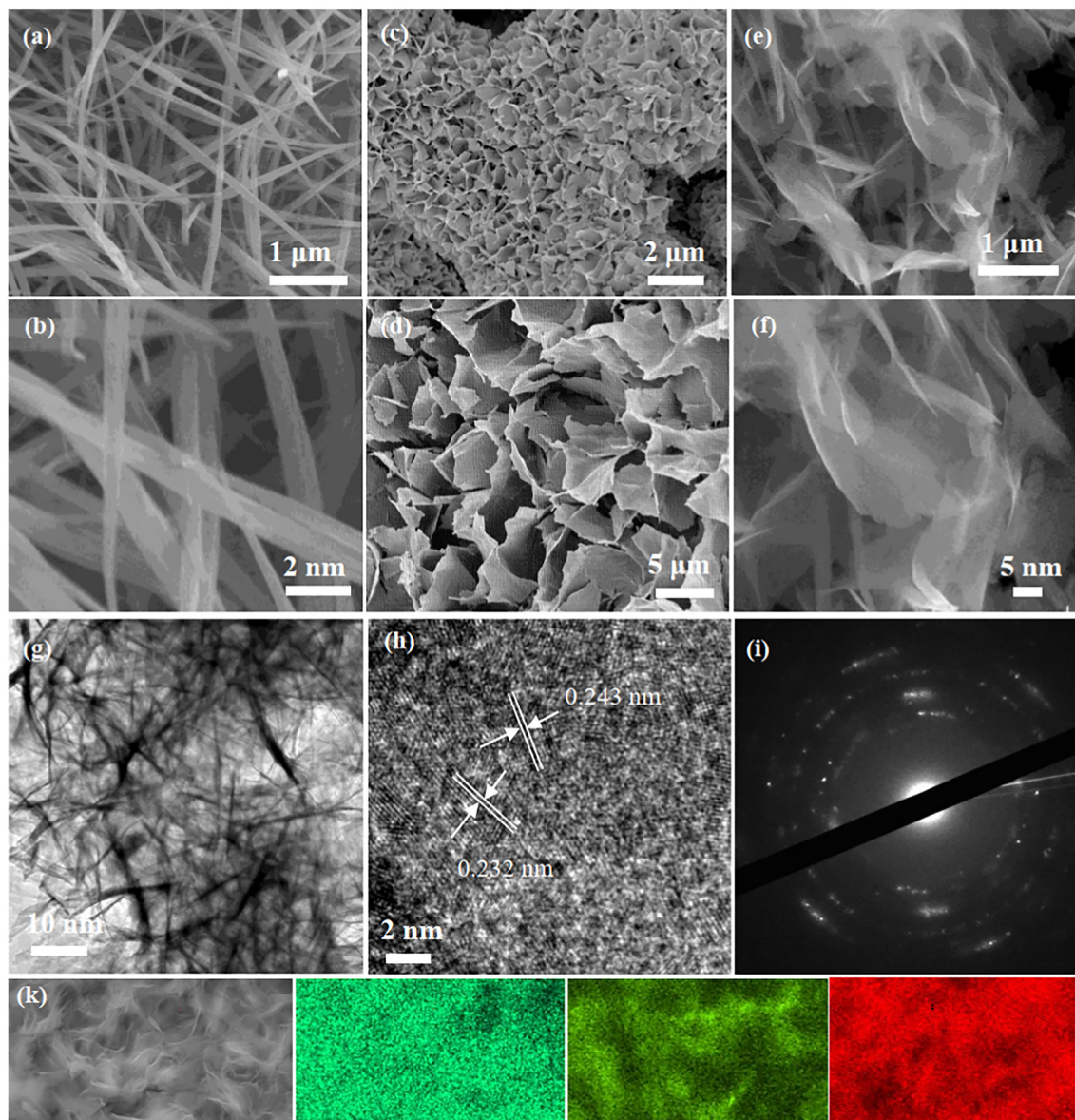


Fig. 3 (a and b) SEM images of ZnCo_2O_4 samples, (c and d) SEM images of Co_3O_4 samples, (e and f) SEM images of $\text{ZnCo}_2\text{O}_4@Co_3O_4$ samples, (g and h) TEM images of $\text{ZnCo}_2\text{O}_4@Co_3O_4$ samples, (i) SAED patterns of $\text{ZnCo}_2\text{O}_4@Co_3O_4$ samples, and (k) elemental mapping of $\text{ZnCo}_2\text{O}_4@Co_3O_4$ products.

originated from the Ni foam, as shown in Fig. 2a. The 2θ value at 31.2° , 43.2° , 59.3° and 65.1° can be assigned to the (220), (311), (511) and (440) crystal planes of ZnCo_2O_4 (JCPDS: 23-1390). The peaks at 28.6° , 47.6° , 56.5° and 88.7° are attributed to Co_3O_4 (JCPDS: 43-1003), corresponding to the (111), (220), (311) and (222) crystal planes, respectively. ZnCo_2O_4 and Co_3O_4 phases can be simultaneously observed in XRD of existing composite materials. It demonstrates that $\text{ZnCo}_2\text{O}_4@Co_3O_4$ product has been successfully produced. The surface element oxidation state of the as-obtained samples can be further analyzed through XPS. Fig. 2b presents the full spectrum of the heterostructure, which proves the existence of the four elements Zn, Co, O, and C. In the Zn 2p spectra (Fig. 2c), the peaks at 1043 and 1022 eV

belong to Zn $2p_{1/2}$ and Zn $2p_{3/2}$ for $\text{ZnCo}_2\text{O}_4@Co_3O_4$ samples.^{25,26} High-resolution Co 2p spectra (Fig. 2d) of $\text{ZnCo}_2\text{O}_4@Co_3O_4$ samples at 781 and 796 eV can be attributed to Co $2p_{3/2}$ and Co $2p_{1/2}$, respectively. Co $2p_{3/2}$ and Co $2p_{1/2}$ can be fitted with two peaks each, the peaks at 779.5 and 794.5 eV can be attributed to Co^{3+} ,²⁷ and the peaks at 782.4 and 796.5 eV can be attributed to Co^{2+} .²⁸ The peaks located at 789.8 and 804.5 eV are related to the vibrational satellite, which can indicate that Co^{2+} and Co^{3+} coexist.²⁹ O 1s spectra (Fig. 2e) can be divided into three peaks, which can be denoted as O1, O2 and O3. The O1 peak at 529.9 eV corresponds to metal–oxygen bonds. The peaks at 531.6 eV and 533.5 eV correspond to surface species and water molecules, respectively.^{30,31}

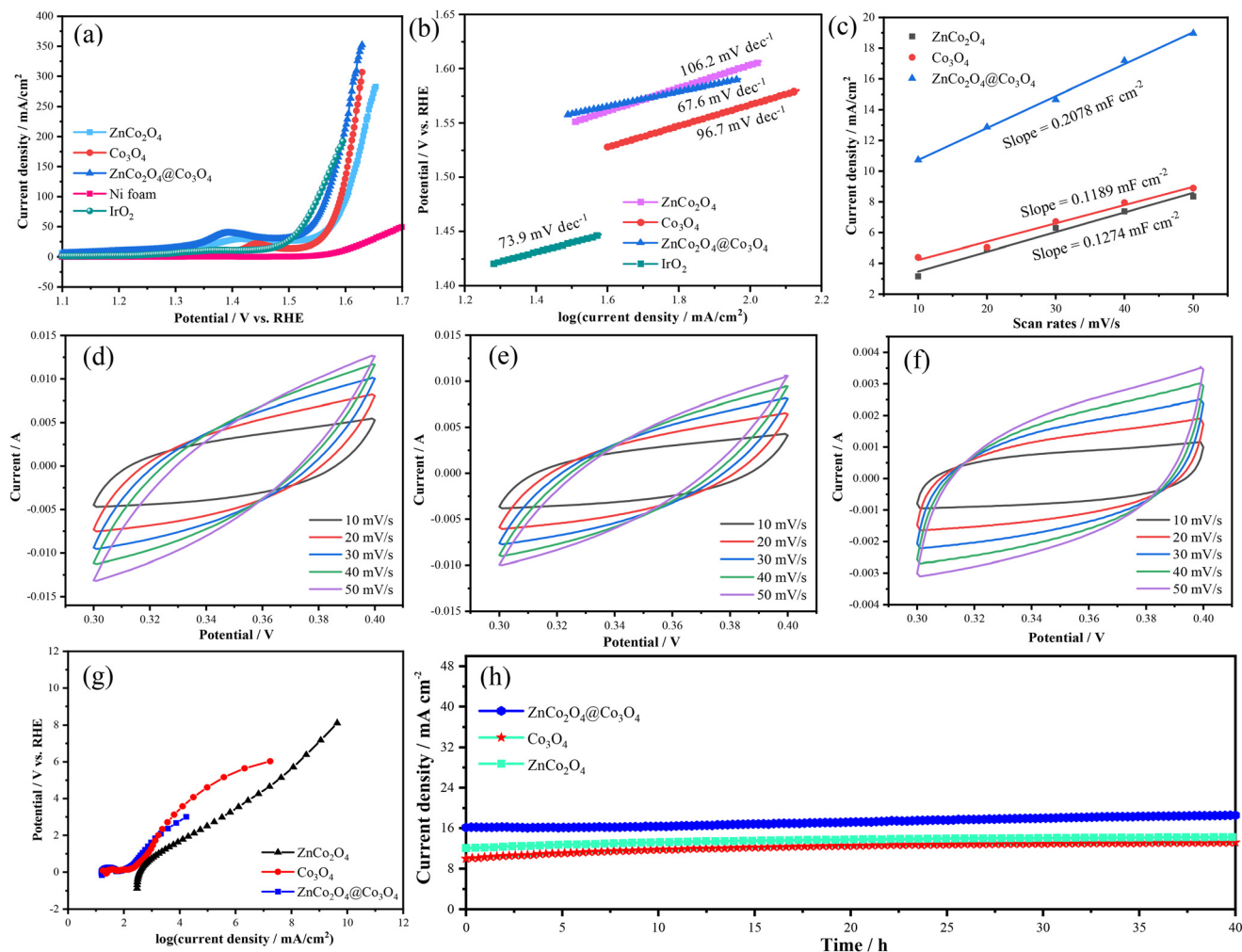


Fig. 4 (a) LSV curves of the electrode materials, (b) Tafel slopes of the electrode materials, (c) double-layer capacitance, CV curves of the (d) ZnCo_2O_4 samples, (e) Co_3O_4 samples, and (f) $\text{ZnCo}_2\text{O}_4@Co_3O_4$ samples, (g) Nyquist plots, and (h) chronoamperometry measurements.

The morphology and structure of the samples were studied by SEM and TEM. The ZnCo_2O_4 sample was observed as shown in Fig. 3a and b, and the surface of the Ni foam was covered by uniformly overlapping nanowires. The average diameter of the product obtained from the high magnification SEM image (Fig. 3b) was 80 nm. Fig. 3c and d show that the morphology of the Co_3O_4 sample is convolved nanosheets, overlapping each other to form a three-dimensional network. As can be seen from Fig. 3e and f, the $\text{ZnCo}_2\text{O}_4@Co_3O_4$ sample follows the morphology of two single samples as the composite of nanowires, and the convolved nanosheets are wrapped around the nanowires, forming a core-shell structure. The results indicated that Co_3O_4 samples were successfully recombined on the ZnCo_2O_4 surface. TEM images of the $\text{ZnCo}_2\text{O}_4@Co_3O_4$ sample are shown in Fig. 3g, and further confirm the morphology of the wire in the slice. In the HRTEM image in Fig. 3h, the lattice spacing of the sample is 0.243 nm and 0.232 nm, respectively, which matches well with the (311) crystal plane of the Co_3O_4 phase and the (222) crystal plane of the ZnCo_2O_4 phase. From the selected electron diffraction pattern

(Fig. 3i), it can be found that the prepared heterostructure is a polycrystalline structure, which is beneficial for enhancing the catalytic active sites, thereby enhancing the electrocatalytic performance. The energy dispersive spectrum (EDS) element diagram of the prepared sample (Fig. 3k) shows the distribution of the Zn, Co, and O elements, indicating that the entire surface composition of the material is uniform.

To evaluate the electrochemical performance of the as-prepared materials, the OER performance was investigated using LSV curves with IR-compensation. Fig. 4a shows that in the range of 1.35–1.45 V *versus* RHE, there is an obvious oxidation peak, which can be attributed to the oxidation of Co and the oxidation of Ni on the nickel foam substrate. For comparison, the LSV curves of an IrO_2 catalyst and nickel foam were also tested. It can be found that the electrocatalytic performance of $\text{ZnCo}_2\text{O}_4@Co_3O_4$ is obviously better than those of the ZnCo_2O_4 and Co_3O_4 samples, and even better than that of the commercial IrO_2 catalyst at high current density, while the influence of nickel foam on the electrocatalytic performance can be ignored. To further study

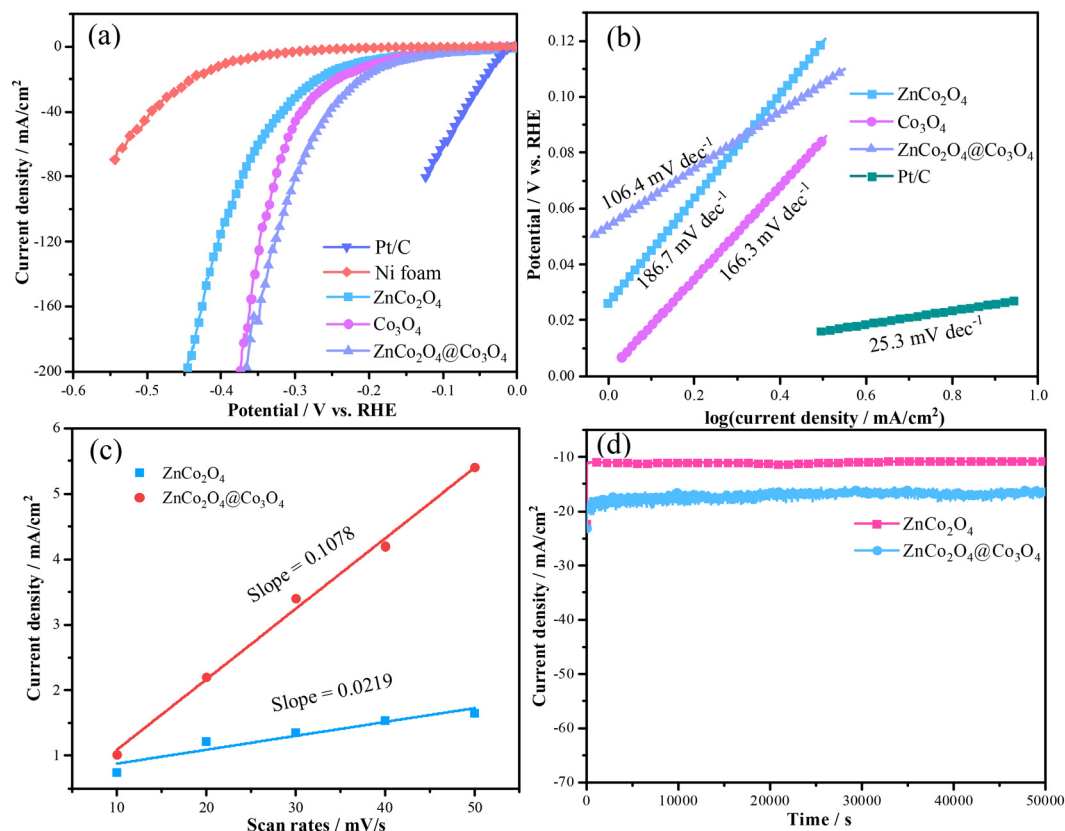


Fig. 5 (a) LSV curves of the electrode materials, (b) Tafel slopes of the electrode materials, (c) double-layer capacitance, and (d) chronoamperometry measurements.

the OER reaction kinetics, the corresponding Tafel slopes are shown in Fig. 4b. The Tafel slope of $\text{ZnCo}_2\text{O}_4@Co_3O_4$ (67.6 mV dec^{-1}) is lower than those of ZnCo_2O_4 ($106.2 \text{ mV dec}^{-1}$), Co_3O_4 (96.7 mV dec^{-1}) and IrO_2 (73.9 mV dec^{-1}). To estimate the intrinsic activity of the catalyst, the electrochemical double-layer capacitance was obtained from the electrochemical double-layer capacitance (Fig. 4c). The measured CV curves all exhibit approximately rectangular shapes (Fig. 4d-f). Compared with ZnCo_2O_4 and Co_3O_4 , the $\text{ZnCo}_2\text{O}_4@Co_3O_4$

sample has a larger ECSA of $0.2078 \text{ mF cm}^{-2}$. To investigate the charge transfer ability of the prepared catalysts, EIS tests were performed (Fig. 4g). In the high frequency region, the $\text{ZnCo}_2\text{O}_4@Co_3O_4$ sample has the smallest semicircular arc representing the charge transfer resistance, which indicates that the synthesis of the composite material effectively improves the charge transfer kinetics. The $i-t$ tests were used to evaluate the electrochemical stability, as shown in Fig. 4h. Compared to ZnCo_2O_4 and Co_3O_4 , $\text{ZnCo}_2\text{O}_4@Co_3O_4$ shows

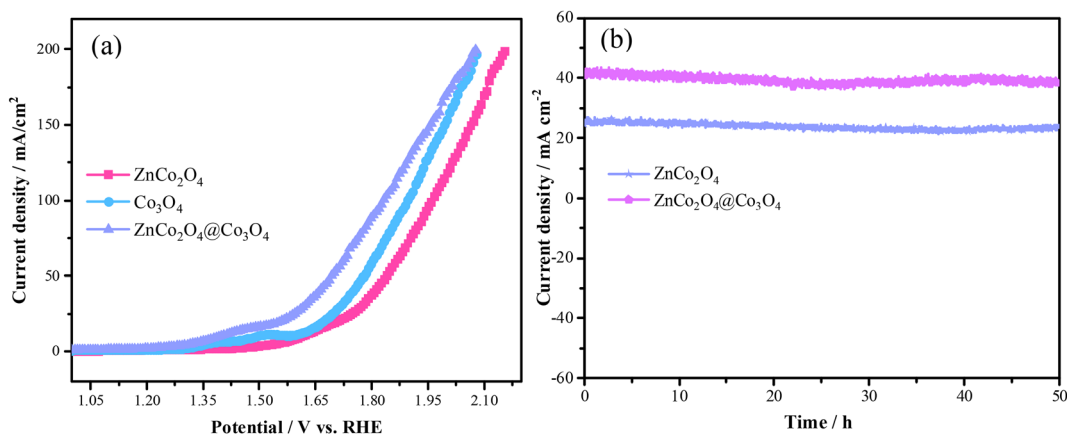


Fig. 6 (a) LSV curves of the electrode materials and (b) chronoamperometry measurements.

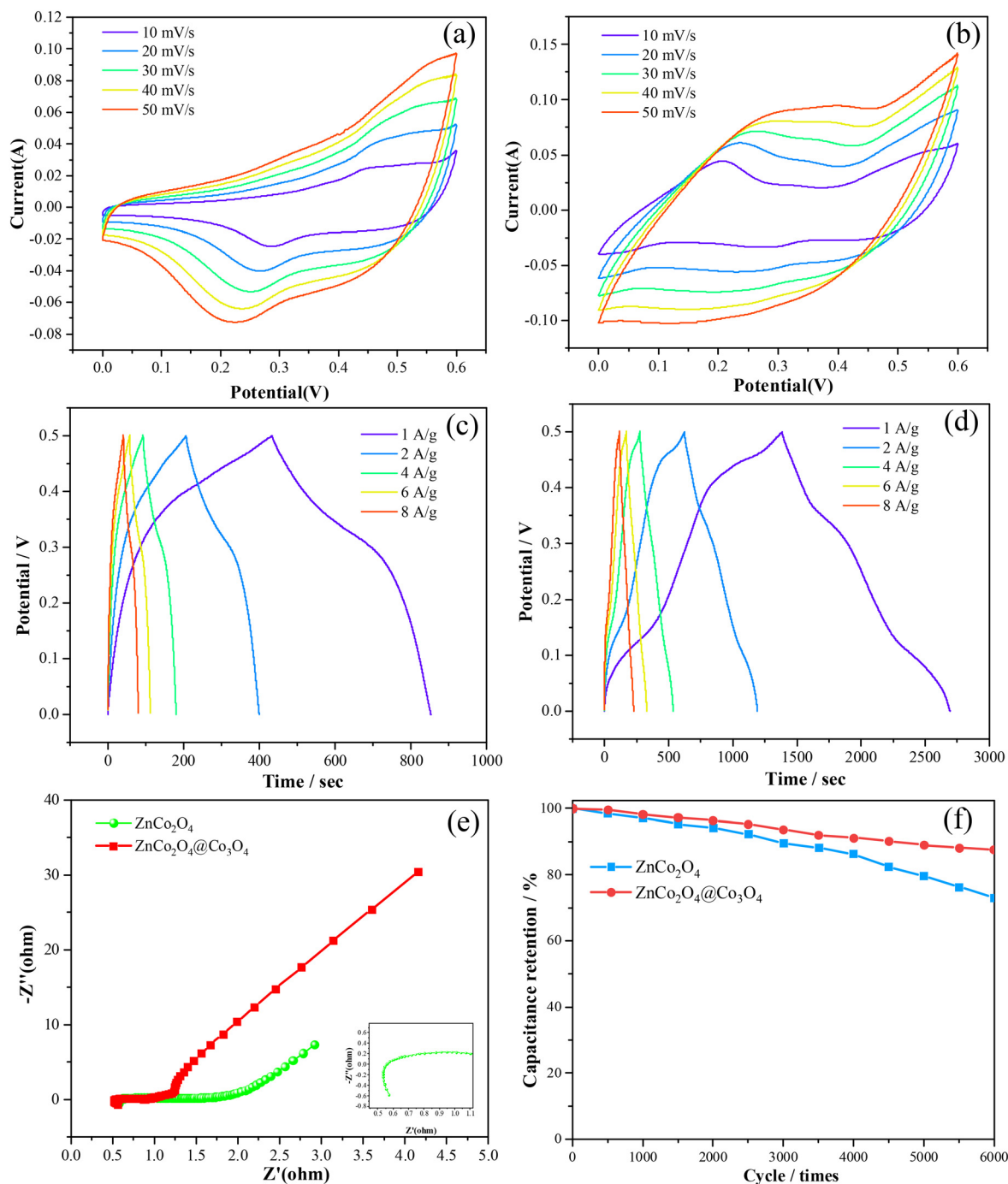


Fig. 7 (a) CV curves of ZnCo_2O_4 , (b) CV curves of $\text{ZnCo}_2\text{O}_4@Co_3O_4$ samples, (c) GCD curves of ZnCo_2O_4 , (d) GCD curves of $\text{ZnCo}_2\text{O}_4@Co_3O_4$, (e) Nyquist plots, and (f) cycling stability.

long-term stability after 40 h at higher current density. The corresponding cycles are monitored by SEM and XPS as shown in Fig. S2 and S3.† Fig. S2(a and b)† show the SEM images of the prepared sample after cycling. It can be found that the as-prepared sample is composed of a large number of nanosheets. Compared with the samples before the cycle, it was found that the morphology of the samples did not change, which confirmed that the prepared samples possess excellent structural stability. XPS was then employed to

further investigate the structural characteristics. The survey spectra in Fig. S3a† confirms that the four elements Zn, Co, O and C can be found throughout the whole sample. Fig. S3b† shows the Co 2p spectrum. The peaks located at 789.6 and 804.6 eV belong to the related Co^+ species. The binding energies of 781.3 and 785.4 eV can be indexed to Co^{3+} . Two satellites reveal the co-existence of the $\text{Co}^{3+}/\text{Co}^{2+}$ peaks.^{32,33} The binding energies of 1021.5 and 1044.2 eV can be ascribed to Zn 2p_{3/2} and Zn 2p_{1/2} (Fig. S3c†).^{34,35} The O 1s spectra (Fig.

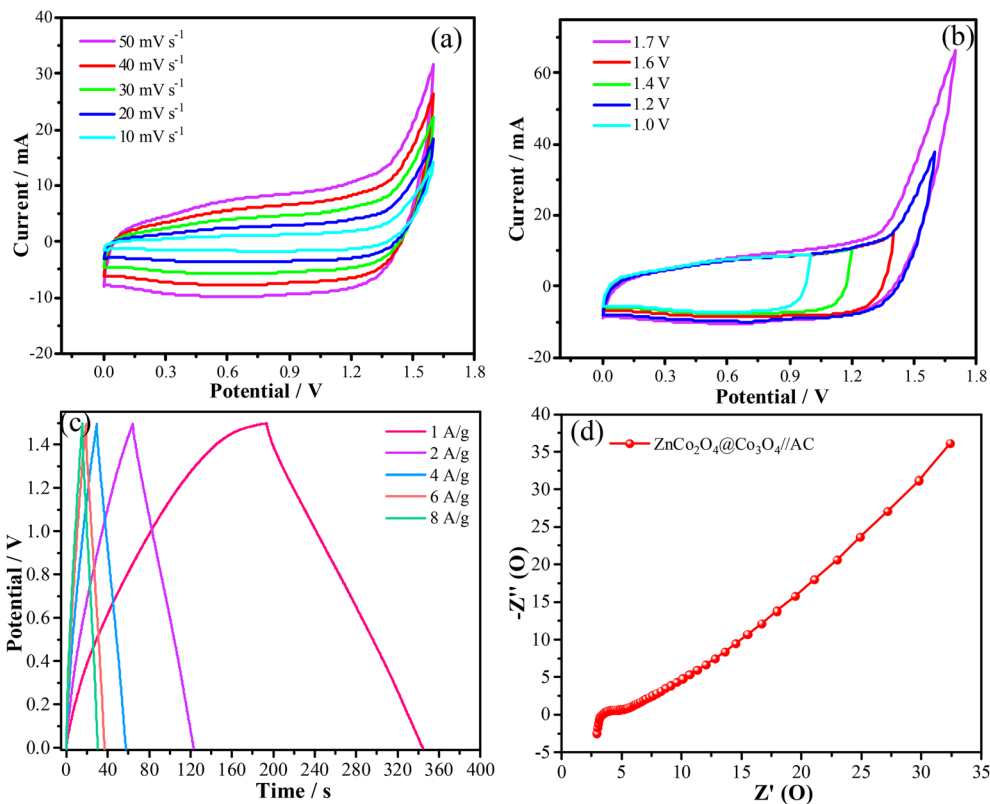


Fig. 8 (a) CV curves of the as-prepared device, (b) CV curves with different voltages, (c) GCD curves, and (d) Nyquist plot of the device.

S3d \uparrow) exhibit three distinct peaks, labeled as O1, O2, and O3. The O1 peak at 531.1 eV corresponds to metal–oxygen bonds, while the peaks at 533.2 eV and 534.5 eV correspond to surface species and water molecules, respectively.^{36,37}

In Fig. 5a, the ZnCo₂O₄@Co₃O₄ electrode shows a lower overpotential (166 mV) than that of single ZnCo₂O₄ (224 mV), Co₃O₄ (198 mV) and Ni foam (391 mV) samples at a current density of 10 mA cm⁻². This indicates that ZnCo₂O₄ and Co₃O₄ phases possess a synergistic effect. And the contribution of nickel foam to the performance is negligible. The Tafel slope was achieved by combining the LSV curve with the Tafel equation as follows:^{38,39}

$$\eta = a + b \log j \quad (1)$$

where η is the overpotential, a is a constant value, b is the Tafel slope, and j is the current density. The kinetics of electron transfer on the catalyst surface during the HER was studied using the Tafel slope. As shown in Fig. 5b, the ZnCo₂O₄@Co₃O₄ catalyst shows a smaller Tafel slope (106.4 mV dec⁻¹) than that of ZnCo₂O₄ (186.3 mV dec⁻¹) and Co₃O₄ (166.7 mV dec⁻¹). This indicates that the heterostructure of ZnCo₂O₄@Co₃O₄ accelerates the electron and ion transport and improves the reactivity of the HER. In addition, the corresponding TOF values are presented in Fig. S1.† Fig. 5c shows the ion diffusion rates of ZnCo₂O₄@Co₃O₄ and ZnCo₂O₄ samples. The slope value of the ZnCo₂O₄@Co₃O₄ electrode (0.1078 mF cm⁻²) is higher than that of the pure ZnCo₂O₄

sample (0.0219 mF cm⁻²), which demonstrates that the heterostructure benefits the rapid transport of OH⁻. Then, the HER cycling stability of ZnCo₂O₄@Co₃O₄ and ZnCo₂O₄ electrode materials was studied. The catalysts show a superior stability at a current density of 20 mA cm⁻² for 50 000 s (Fig. 5d). At the same time, we also compared the electrocatalytic performance of the prepared product with the reported catalysts.

Based on the OER and HER electrocatalytic test results, the heterostructured ZnCo₂O₄@Co₃O₄ has excellent electrocatalytic performance, so a two-electrode system was constructed to study its practical application as an electrode material. A comparison of the water splitting ability can be observed in Fig. 6a, where the cell voltage of ZnCo₂O₄@Co₃O₄ is much smaller than that of ZnCo₂O₄ and shows a higher current density. The cell voltage of the ZnCo₂O₄@Co₃O₄ electrocatalyst is only 1.67 V (50 mA cm⁻²) compared to the cell voltage of ZnCo₂O₄ (1.82 V) and Co₃O₄ (1.79 V). The stability test of long-term water splitting is shown in Fig. 6b. The current values of the as-prepared catalysts remained unchanged during continuous water splitting, indicating their excellent long-term stability, and the composite catalysts exhibited stability at high current densities.

Fig. 7a presents the CV curve of the prepared ZnCo₂O₄ sample, indicating an increase in the curve area with an increase in the scan rate. Additionally, distinct oxidation–reduction peaks can be observed. Fig. 7b shows the CV curve of the composite ZnCo₂O₄@Co₃O₄ electrode material,

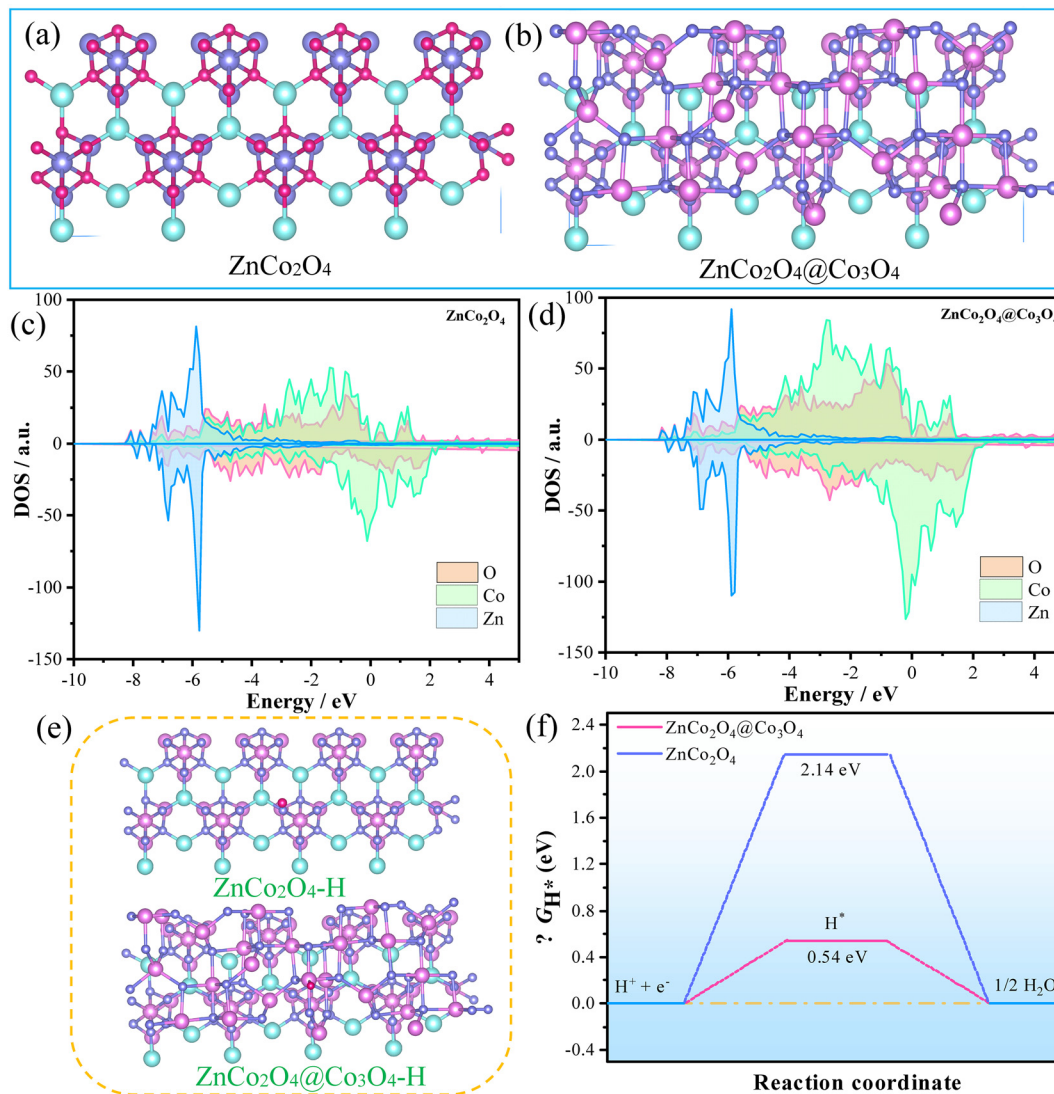


Fig. 9 (a and b) Structural models of ZnCo₂O₄ and ZnCo₂O₄@Co₃O₄ samples, (c and d) the projected density of states, (e) H adsorption structural models of the ZnCo₂O₄ and ZnCo₂O₄@Co₃O₄ samples, and (f) calculated free energy diagrams of H adsorption of different components.

revealing larger current density and curve area, indicating the superior electrochemical performance of the composite material. From Fig. 7c, it can be observed that the prepared electrode material exhibits a symmetrical charge-discharge curve, with a discharge time of 405 s corresponding to a specific capacitance of 405 C g⁻¹. Fig. 7d presents the charge-discharge curve of the composite material, demonstrating a discharge time of 1316 s, indicating a high specific capacitance of 1316 C g⁻¹. The impedance spectrum (Fig. 7e) reveals that the composite material possesses lower equivalent resistance and higher charge transfer capability. Cycling stability (Fig. 7f) plays a crucial role in the potential applications of electrode materials. It can be observed that the composite material exhibits excellent cycling stability, with a capacity retention rate of 87.15% after 6000 cycles, significantly higher than that of the individual electrode material (72%).

To evaluate the practical applications of the fabricated electrode materials, we constructed a hybrid capacitor utilizing ZnCo₂O₄@Co₃O₄ as the positive electrode and activated carbon (AC) as the negative electrode. The cyclic voltammetry (CV) curves were obtained at different scan rates, as depicted in Fig. 8a. With increasing scan rate, the integrated area consistently increases while maintaining a nearly rectangular shape, indicating favorable capacitive properties of the asymmetric supercapacitor (ASC). Additionally, Fig. 8b illustrates the CV curves at different voltage windows, showing consistent shapes despite the varying voltage ranges. This observation indicates the remarkable operational stability of the ASC under different voltage conditions. The discharge curves of the ASC are presented in Fig. 8c, with corresponding discharges of 151.6 s, 57.2 s, 26.3 s, 18.6 s and 17.7 s at 1 A g⁻¹, 2 A g⁻¹, 4 A g⁻¹, 6 A g⁻¹ and 8 A g⁻¹, respectively. Electrochemical impedance spectroscopy (EIS) tests (Fig. 8d) reveal an R_s value of 2.9 Ω

for the device. The device achieves a maximum energy density of 47.3 W h kg^{-1} at a power density of 1126 W kg^{-1} .

Density functional theory (DFT) is commonly used to calculate the surface adsorption energy and partial densities of states (PDOS and TDOS) of electrocatalysts and hydrogen atoms.⁴⁰ The crystal cell models of ZnCo_2O_4 and $\text{ZnCo}_2\text{O}_4@\text{Co}_3\text{O}_4$ samples are shown in Fig. 9(a and b). The partial densities of states of the electrocatalysts were calculated to investigate the intrinsic electronic changes. The DOS analysis reveals that the heterostructure is in the metallic state, as depicted in Fig. 9(c and d). This indicates that the $\text{ZnCo}_2\text{O}_4@\text{Co}_3\text{O}_4$ sample exhibits an enhanced carrier density near the Fermi energy level. Previous studies have shown that the higher the electron density at the Fermi level, the higher the conductivity of the catalyst. The change in Gibbs free energy of adsorption (ΔG) is often used to evaluate the hydrogen evolution reaction (HER) activity of catalysts, with the red atoms representing the adsorption site (Fig. 9e). Theoretically, a ΔG value close to 0 eV signifies an intermediate H adsorption and desorption strength for an ideal catalyst. From Fig. 9f, the ΔG° values of H adsorption on ZnCo_2O_4 (202) and $\text{ZnCo}_2\text{O}_4@\text{Co}_3\text{O}_4$ (202) surfaces are 2.14 and 0.54 eV, respectively, which are relatively close to the ideal value.

Conclusion

In summary, hybrid-structure $\text{ZnCo}_2\text{O}_4@\text{Co}_3\text{O}_4$ nanowires are successfully synthesized through hydrothermal synthesis and electrodeposition. As electrocatalysts for water splitting, $\text{ZnCo}_2\text{O}_4@\text{Co}_3\text{O}_4$ can reach a current density of 50 mA cm^{-2} at an overpotential of 278 mV for the OER and 166 mV for the HER, which could be higher than that of single ZnCo_2O_4 and Co_3O_4 . At the same time, $\text{ZnCo}_2\text{O}_4@\text{Co}_3\text{O}_4$ samples also exhibit a cell voltage of 1.67 V and superior durability for 50 h. The as-fabricated product exhibits a specific capacitance of 1316 F g^{-1} at 1 A g^{-1} . This work offers a novelty design route of core-shell structures, which is helpful for fabrication of hybrid structures for energy conversion.

Conflicts of interest

The authors declare no conflict of interest.

Acknowledgements

This project is supported by the Education Department of Liaoning Province (LJKMZ20221794).

References

- 1 Y. Yang, W. Zhang, Y. Xiao, Z. Shi, X. Cao, Y. Tang and Q. Gao, *Appl. Catal., B*, 2019, **242**, 132–139.
- 2 X. F. Li, L. Zhang, H. R. Chai, Y. B. Zhang, R. Wang, M. Xie, Y. C. Xu, J. R. Chen and Y. Jiao, *J. Colloid Interface Sci.*, 2023, **632**, 186–195.
- 3 P. Liu, R. Lv, Y. He, B. Na, B. Wang and H. Liu, *J. Power Sources*, 2019, **410**, 137–142.
- 4 S. K. Li, H. R. Chai, L. Zhang, Y. C. Xu, Y. Jiao and J. R. Chen, *J. Colloid Interface Sci.*, 2023, **642**, 235–245.
- 5 Z. Lu, B. Wang, Y. Hu, W. Liu, Y. Zhao, R. Yang, Z. Li, J. Luo, B. Chi, Z. Jiang, M. Li, S. Mu, S. Liao, J. Zhang and X. Sun, *Angew. Chem., Int. Ed.*, 2019, **58**, 2622–2626.
- 6 S. S. Xiong, M. X. Lin, L. D. Wang, S. Liu, S. T. Weng, S. Y. Jiang, Y. C. Xu, Y. Jiao and J. R. Chen, *Appl. Surf. Sci.*, 2021, **546**, 149064.
- 7 J. W. Zhu and S. C. Mu, *Inorg. Chem. Front.*, 2023, **10**, 2220–2225.
- 8 Z. W. Li, W. T. Zhang, M. Tao, L. G. Shen, R. J. Li, M. J. Zhang, Y. Jiao, H. C. Hong, Y. C. Xu and H. J. Lin, *Chem. Eng. J.*, 2022, **435**, 134804.
- 9 Z. Wang, H. Liu, R. Ge, X. Ren, J. Ren, D. Yang, L. Zhang and X. Sun, *ACS Catal.*, 2018, **8**, 2236–2241.
- 10 L. Shen, J. Wang, G. Xu, H. Li, H. Dou and X. Zhang, *Adv. Energy Mater.*, 2015, **5**, 22284–22291.
- 11 D. Du, R. Lan, J. Humphreys, W. Xu, K. Xie, H. Wang and S. Tao, *J. Electrochem. Soc.*, 2017, **164**, 2881–2888.
- 12 J. Chen, J. Xu, S. Zhou, N. Zhao and C. P. Wong, *Nano Energy*, 2016, **25**, 193–202.
- 13 (a) S. M. Pawar, B. S. Pawar, P. T. Babar, A. T. A. Ahmed, H. S. Chavan, Y. Jo, S. Cho, J. Kim, B. Hou, A. I. Inamdar, S. Cha, J. H. Kim, T. G. Kim, H. Kim and H. Im, *Appl. Surf. Sci.*, 2019, **470**, 360–367; (b) Z. Chen, C. X. Kronawitter, Y.-W. Yeh, X. Yang, P. Zhao, N. Yao and B. E. Koel, *J. Mater. Chem. A*, 2017, **5**, 842–850.
- 14 H. Khani, N. S. Grundish, D. O. Wipf and J. B. Goodenough, *Adv. Energy Mater.*, 2019, **10**, 1903215.
- 15 Q. Wang, L. Zhu, L. Sun, Y. Liu and L. Jiao, *J. Mater. Chem. A*, 2015, **3**, 982–985.
- 16 B. Guan, D. Guo, L. Hu, G. Zhang, T. Fu, W. Ren, J. Li and Q. Li, *J. Mater. Chem. A*, 2014, **2**, 16116–16123.
- 17 B. Liu, B. Liu, Q. Wang, X. Wang, Q. Xiang, D. Chen and G. Shen, *ACS Appl. Mater. Interfaces*, 2013, **5**, 10011–10017.
- 18 H. Wu, Z. Lou, H. Yang and G. Z. Shen, *Nanoscale*, 2014, **29**, 1799–1803.
- 19 G. M. Tomboc, H. S. Jadhav and H. Kim, *Chem. Eng. J.*, 2016, **6**, 470–476.
- 20 Y. F. Zhao, W. Ran, J. He, Y. Z. Huang, Z. F. Liu, W. Liu, Y. F. Tang, D. W. Gao and F. M. Gao, *Small*, 2015, **11**, 1310–1319.
- 21 X. Xiao, G. Wang, M. Zhang, Z. Wang, R. Zhao and Y. Wang, *Ionics*, 2018, **24**, 2435–2443.
- 22 H. Li, L. Wang, Y. Guan, Y. Su, J. Mu, H. Che, A. Liu and Z. C. Guo, *Appl. Phys. A: Mater. Sci. Process.*, 2018, **124**, 485.
- 23 Y. Pan, H. Ren, H. Du, F. Cao, Y. Jiang, H. Du and D. Chu, *J. Mater. Chem. A*, 2018, **6**, 22497–22502.
- 24 H. H. Pham, M.-J. Cheng, H. Frei and L.-W. Wang, *ACS Catal.*, 2016, **6**, 5610–5617.
- 25 Z. Y. Gao, L. C. Zhang, J. L. Chang, Z. Wang, D. P. Wu, F. Xu, Y. M. Guo and K. Jiang, *Appl. Surf. Sci.*, 2018, **442**, 138–147.
- 26 Z. Q. Zhang, X. Y. Zhang, Y. Feng, X. F. Wang, Q. S. Sun, D. Y. Yu, W. M. Tong, X. D. Zhao and X. Y. Liu, *Electrochim. Acta*, 2018, **260**, 823–829.

- 27 Y. Zhu, T. F. Cai, H. P. Rui, X. Y. Gu, X. Q. Mu, Y. Tong, H. B. Duan, C. Y. Chen, S. L. Liu and S. C. Mu, *J. Alloys Compd.*, 2022, **889**, 161704.
- 28 (a) J. Li, P. Xu, R. Zhou, R. Li, L. Qiu, S. P. Jiang and D. Yuan, *Electrochim. Acta*, 2019, **299**, 152–162; (b) H. B. Tao, J. Zhang, J. Chen, L. Zhang, Y. Xu, J. G. Chen and B. Liu, *J. Am. Chem. Soc.*, 2019, **141**, 13803–13811.
- 29 M. Yu, X. Q. Mu, W. T. Meng, Z. Y. Chen, Y. Tong, Y. Ge, S. Y. Pang, S. J. Li, S. L. Liu and S. C. Mu, *Renewables*, 2023, DOI: [10.31635/renewables.023.202300025](https://doi.org/10.31635/renewables.023.202300025).
- 30 L. Yang, D. Liu, S. Hao, R. Kong, A. M. Asiri, C. Zhang and X. Sun, *J. Mater. Chem. A*, 2017, **5**, 7305–7308.
- 31 M. García-Mota, M. Bajdich, V. Viswanathan, A. Vojvodic, A. T. Bell and J. K. Nørskov, *J. Phys. Chem. C*, 2012, **116**, 21077–21082.
- 32 M. Huang, W. Liu, L. Wang, J. Liu, G. Chen, W. You, J. Zhang, L. Yuan, X. Zhang and R. Che, *Nano Res.*, 2020, **13**, 810.
- 33 Z. Wang, H. Wang, S. Ji, X. Wang, B. G. Pollet and R. Wang, *J. Power Sources*, 2020, **446**, 227348.
- 34 D. Song, J. Zhu, J. Li, T. Pu, B. Huang, C. Zhao, L. Xie and L. Chen, *Electrochim. Acta*, 2017, **257**, 455–464.
- 35 J. Sun, P. Zan, L. Ye, X. Yang and L. Zhao, *J. Mater. Chem. A*, 2017, **5**, 9815–9823.
- 36 J. Yu, Q. Cao, Y. B. Li, X. Long, S. H. Yang, J.-K. Clark, M. Nakabayashi, N. Shibata and J.-J. Delaunay, *ACS Catal.*, 2019, **9**, 1605–1611.
- 37 S. Dou, C. L. Dong, Z. Hu, Y. C. Huang, J. L. Chen, L. Tao, D. Yan, D. Chen, S. Shen, S. Chou and S. Wang, *Adv. Funct. Mater.*, 2017, **27**, 1702546.
- 38 J. Wang, J. Liu, B. Zhang, H. Wan, Z. Li, X. Ji, K. Xu, C. Chen, D. Zha and L. Miao, *Nano Energy*, 2017, **42**, 98–105.
- 39 D. P. Xue, J. Q. Cheng, H. C. Xia, B. A. Lu, P. F. Yuan, C. C. Yang, C. L. Dong, H. Z. Zhang, F. Y. Shi, S. C. Mu, J. S. Hu, S. G. Sun and J. N. Zhang, *Adv. Funct. Mater.*, 2022, **32**, 2113191.
- 40 D. Chen, R. H. Lu, R. H. Yu, Y. H. Dai, H. Y. Zhao, D. L. Wu, P. Y. Wang, J. W. Zhu, Z. H. Pu, L. Chen, J. Yu and S. C. Mu, *Angew. Chem.*, 2022, **61**, e202208642.